Particle simulations of efficient fast electron generation near the cutoff layer of an electrostatic wave

S. J. Karttunen and T. J. H. Pättikangas
VTT Energy, Association Euratom–TEKES, P. O. Box 1604, FIN-02044 VTT, Finland

T. J. J. Tala
Advanced Energy Systems, Helsinki University of Technology, Association Euratom–TEKES, P. O. Box 2200, FIN-02015 HUT, Finland

R. A. Cairns
School of Mathematical and Computational Sciences, University of St. Andrews, St. Andrews, Fife, KY16 9SS, United Kingdom

(Received 24 June 1996; revised manuscript received 20 May 1997)

Fast electron generation near the cutoff of an electrostatic plasma wave is investigated by particle-in-cell simulations and test particle calculations. Intense electron plasma waves which are excited in an underdense plasma region propagate up the density gradient until they are reflected from the cutoff layer. The density gradient affects the fast electron generation by the wave considerably. At low densities, the phase velocity is fairly close to the thermal distribution, which leads to wave-particle interactions with a large electron population. The trapped electrons are accelerated by the electron plasma wave with increasing phase velocity resulting in a very large and energetic population behind the cutoff layer. Since the accelerating electrons receive energy, the wave must be damped. A simple model based on the conservation of the energy of the wave and the trapped electrons is developed to describe the damping mechanism.
[S1063-651X(97)00409-1]

PACS number(s): 52.40.Nk, 52.35.Fp

I. INTRODUCTION

Superthermal electrons play an important role in many fusion-related plasma experiments. One source of fast electrons in plasmas is nonlinear or quasilinear wave-particle interactions. In tokamak experiments, fast electrons are generated by various radio frequency waves used for plasma heating and current drive. In laser fusion, fast electrons are born in wave-particle processes taking place in underdense plasma regions or at critical density layers. Electrostatic plasma waves—for instance, Langmuir or lower hybrid waves—are able to modify the electron velocity distribution around the phase velocity via the Landau resonance. The width of the resonance is determined by the wave spectrum or in the case of a single mode by the amplitude of the wave.

In the so-called beat-wave accelerator [1], large amplitude electron plasma waves form the accelerating field structure for electron and positron beams to reach ultrahigh energies. In laser plasmas, parametric instabilities may generate large amplitude Langmuir waves which produce nonthermal electrons. In magnetized plasmas, waves with high phase velocities generated by the beat-wave coupling or stimulated Raman scattering have been suggested for driving current in tokamaks [2,3]. In current drive, fast electrons are beneficial due to their low collisionality, but in laser fusion they are very damaging in terms of preheating of the pellet core.

Another means of affecting the fast electron generation is to vary the phase velocity of the wave. This occurs, for instance, in the lower hybrid current drive where the fast electron population is much larger than expected from the launched $k_{\|}$ spectrum because of the toroidal upshift which changes the parallel phase velocities [4]. Another example is staged acceleration of electrons by two or more electrostatic waves with different phase velocities. This can occur, for instance, in simultaneous stimulated Raman forward and backward scattering where the electron plasma waves are separated locally [5,6].

The simplest case involving variations in the phase velocity is an electron plasma wave propagating in an inhomogeneous plasma. Small variations in the plasma density may change considerably the phase velocity of a Langmuir wave. At low densities, the phase velocity is fairly close to the thermal distribution, which leads to wave-particle interactions with a large electron population. The trapped electrons are accelerated by the electron plasma wave with an increasing phase velocity resulting in a very large and energetic population behind the cutoff layer.

Intense electron plasma waves are generated, for instance, by parametric instabilities such as the stimulated Raman scattering or the two plasmon decay instability in the underdense laser plasmas or in the beat-wave current drive of tokamak plasmas. Resonance absorption of an electromagnetic wave at the critical density is another example in which large amplitude electron plasma waves and fast electrons are involved. In this case, the Langmuir waves are excited by linear mode conversion. Fast electron energies in resonance absorption remain typically well below those obtained in the stimulated Raman scattering or two plasmon decay. Fast electron generation and damping of an electron plasma wave in the resonance absorption of laser light have recently been analyzed by Vlasov simulations [7].

In this paper we study the acceleration of electrons in an

 © 1997 The American Physical Society

inhomogeneous plasma by an electron plasma wave that is reflected at the cutoff layer. The key factor is the rapidly increasing phase velocity close to the cutoff layer where the wave frequency equals the local plasma frequency. We analyze the fast electron generation by following test electrons in an externally given wave, where the well known Airy pattern of the wave field is used in the equations of motion. The increase in the momentum of the electrons is measured when they travel through the Airy-type wave packet near the cutoff layer.

The fast electron generation is also investigated with self-consistent particle-in-cell (PIC) simulations, where the Langmuir wave is excited by an antenna in an underdense plasma. When the wave is reflected from the cutoff layer, the acceleration of an ensemble of test electrons traveling through the cutoff is investigated. The effect of the steepness of the density gradient on the fast electron energies is studied and compared with analytical estimates.

Since the electrons trapped in the wave potential receive energy when the phase velocity increases, the wave must lose energy and be damped. We will call this mechanism ''drag damping'' because the wave with an increasing phase velocity ''drags'' the electrons to higher velocities. A phenomenological model for the ''drag damping'' is developed by considering conservation of energy of the wave and the trapped electrons. The parameter region where the ''drag damping'' is important is investigated by comparing it with the linear Landau damping. Finally, the phenomenological model is compared with the results of the PIC simulations.

In Sec. II we present briefly the basic features of the Langmuir wave propagation in a density gradient. Simple test particle calculations with an ensemble of electrons are presented in Sec. III. Particle-in-cell simulations of the Langmuir wave excitation in an inhomogeneous plasma and the resulting fast electron generation are analyzed in Sec. IV and Sec. V. The fast electron generation in steep and gentle density gradients is compared in Sec. VI. A simple analytical model for the ''drag damping'' is presented in Sec. VII. Finally, the results are summarized and discussed in Sec. VIII.

II. REFLECTION OF AN ELECTRON PLASMA WAVE

Short wavelength electron plasma waves $\mathbf{E}(\mathbf{k},\omega)$ are fairly heavily damped and they can only propagate short distances. At longer wavelengths ($k\lambda_D<0.3$, where λ_D is the Debye length), the weak Landau damping allows growth of the driven wave to higher amplitudes and easier propagation of the plasma wave. A propagating plasma wave is very sensitive to density variations when the wave travels nearly parallel to the density gradient. A small change in the plasma density has a strong influence on the phase velocity of the wave. For the waves traveling up the density gradient, the phase velocity increases rapidly near the cutoff layer, and the wave is reflected. The Landau damping of the reflected plasma wave increases during its propagation, which leads to full absorption of the wave energy in the low density region.

We assume a linear density ramp $n(x)=[n_c-n(0)](x/x_c)+n(0)$, where n_c is the critical or the cutoff density of the electron plasma wave, i.e., $\omega_p(x_c)=\omega$. Taking harmonic time dependence and Fourier transforming in y direction we obtain from the wave equation for the amplitude $\delta n_e(x)$ the well known Airy equation [8,9]

$$\left(\frac{d^2}{dx^2}+k_x^2(x)\right)\delta n_e(x)=0, \tag{1}$$

where $k_x^2(x)=k_0^2(1-x/x_c)-k_y^2$ and $k_0^2=k_y^2+k_x^2(0)=[\omega^2-\omega_p^2(0)]/3v_e^2$ and v_e is the thermal velocity. The solution can be written in terms of the Airy functions.

The Airy function solution of Eq. (1) includes both the incoming and the reflected wave component and a rapidly decreasing part in the evanescent region behind the cutoff layer. If the wave propagates along the density gradient ($k_y=0$), we find from the linear dispersion relation $v_{\rm ph}=\omega/k(x)\to\infty$ when $x\to x_c$, which corresponds to the mode cutoff and the reflection of the wave. In a steady state, the Airy field pattern forms a localized wave packet which interacts with the electrons traveling through it.

III. TEST PARTICLE SIMULATIONS

We analyze the electron behavior with simple test particle simulations using an external prescribed wave field. The electric field moves the electrons but is not affected by them. We assume an electron plasma wave which is traveling parallel to the density gradient in a linear density profile. The phase velocity of the plasma wave is changing during propagation so that the wave-particle resonance condition $v=\omega/k$ covers a range of values in the velocity space. This has a clear effect on the fast electron generation around the cutoff layer.

The normalized equations of motion for relativistic test electrons are given by

$$\frac{d\xi}{d\tau}=p(1+p^2)^{-1/2}, \tag{2}$$

$$\frac{dp}{d\tau}=\frac{q_eE(\xi,\tau)}{m_e\omega c}, \tag{3}$$

where q_e is the electron charge, m_e is the electron mass, E is the electric field of the wave, and $\tau=\omega t$, $\xi=\omega x/c$, and $p=\gamma v/c$ are the normalized time, space, and momentum, respectively. The relativistic Lorentz factor is $\gamma=[1-(v/c)^2]^{-1/2}$. The electric field $E(\xi,\tau)$ for the electron plasma wave in Eq. (2) is taken to be the Airy-type pattern $E(\xi,\tau)=E_0{\rm Ai}\{(k_0x_c)^{2/3}(\xi/\xi_c-1)\}\cos\tau$, where we have assumed $k_y=0$.

We assume that the plasma wave is excited at densities from $n(0)/n_c=0.5$ to 0.6 with an initial phase velocity of $v_{\rm ph}\simeq 0.33c$ which corresponds to $v_{\rm ph}\simeq 2.5v_e$ when the electron temperature is $T_e=10$ keV. Figure 1(a) illustrates the normalized electric field $q_eE/m_e\omega c$ of a reflecting plasma wave in an inhomogeneous plasma. The cutoff layer is at $\xi=180$ showing the Airy enhancement of the electric field. The enhancement of the wavelength near the cutoff is clearly seen in the field pattern of Fig. 1(a).

Typical behavior of the electron momentum is shown in Fig. 1(b). The initial momentum is $p_{\rm in}=0.3$, which is inside the trapping width of the wave potential. The trapped electron performs bounce motion in the wave potential and is accelerated with the increasing phase velocity. The dashed

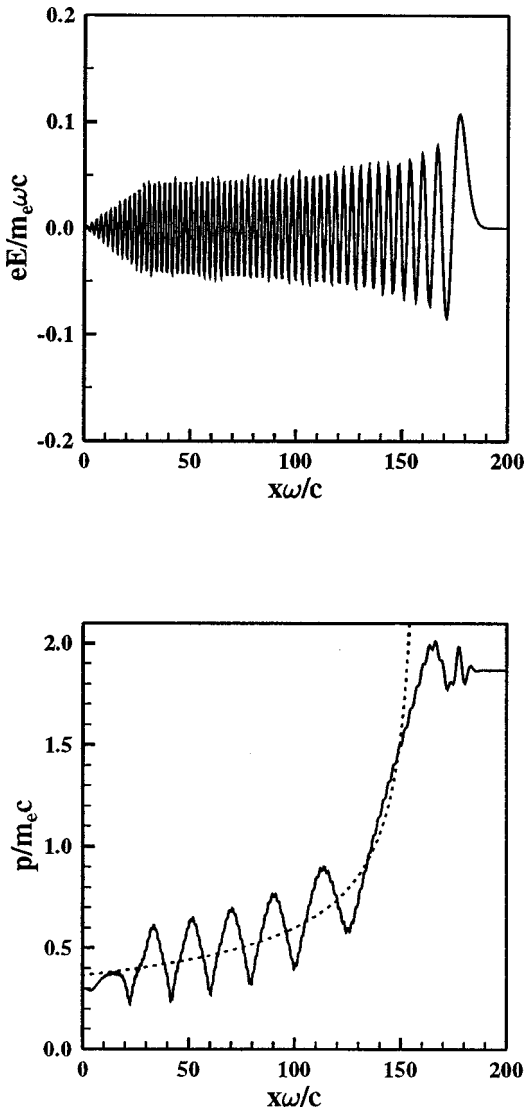

FIG. 1. (a) Airy function solution of the electron plasma wave in a linear density profile, and (b) a trajectory of a typical single electron traveling through the same wave packet. Dashed line shows the phase velocity of the plasma wave obtained from the linear Bohm-Gross dispersion relation.

line gives the phase velocity of the electron plasma wave according to the linear Bohm-Gross dispersion relation. The bounce-averaged electron velocity follows closely the phase velocity until the electron escapes from the wave potential with a larger momentum of $p_{\rm out}\simeq 1.8$.

The maximum velocity of the accelerated electrons can be estimated from the largest wavelength in the Airy pattern. We estimate $\lambda_{\rm max}/2\simeq x_1-x_2$, where x_1 and x_2 are the first and the second zero of the field to the left of the cutoff layer. The zeroes of the Airy function occur at $a_1\simeq -2.34$ and $a_2\simeq -4.09$, where we have defined $\mathrm{Ai}(a_s)=0$, see Ref. [10]. The maximum wavelength is approximately

$$\lambda_{\rm max}\simeq 2(a_1-a_2)(x_c k_0)^{1/3}/k_0, \tag{4}$$

and the corresponding minimum wave number is $k_{\rm min}\simeq 1.8(k_0 x_c)^{-1/3}k_0$.

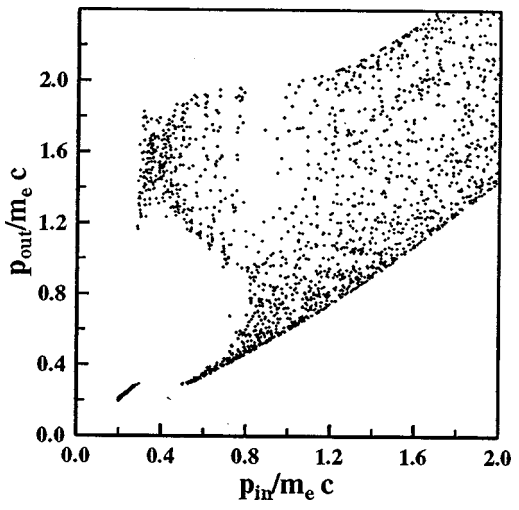

FIG. 2. Final momenta versus initial momenta of an ensemble of 2000 test electrons traveling up the density gradient through the Airy-type wave packet.

The ratio of the phase velocities at the cutoff layer and at $x=0$ is approximately

$$\frac{v_{\rm ph}(x_c)}{v_{\rm ph}(0)}\simeq 0.56(k_0 x_c)^{1/3}. \tag{5}$$

The interpretation of this result is simple. The smaller the initial phase velocity, the larger the enhancement of the phase velocity near the cutoff layer. The longer the plasma with the linear density ramp, the higher the phase velocity near the cutoff layer.

Figure 2 shows the final momenta $p_{\rm out}$ of an ensemble of 2000 test electrons traveling through the Airy-type wave packet of Fig. 1(a) from the low density side. Test electrons are evenly distributed between the initial momenta $p_{\rm in}=0.1$ and 2. A remarkable feature is that practically all electrons between $p_{\rm in}=0.3$ and 0.5 are accelerated to very high momenta around $p_{\rm out}=1.5$. The enhancement of the momentum of these electrons is $p_{\rm out}/p_{\rm in}\simeq 3.8$. The corresponding enhancement of the phase velocity estimated from Eq. (5) is somewhat larger: $v_{\rm ph}(x_c)/v_{\rm ph}(0)=4.6$.

The effect shown in Fig. 2 is emphasized in a Maxwellian plasma which has very few particles above $p=0.5$. Electron velocity distribution behind the cutoff layer in a Maxwellian plasma is illustrated in Fig. 3. It is obtained by assuming a Maxwellian distribution at the low density boundary so that the initial phase velocity is $v_{\rm ph}\simeq 2.5v_e$. The Maxwellian electrons travel through the same Airy-type wave packet as in the previous case. The resulting velocity distribution has an isolated bump on the tail rather than a plateau because the accelerating wave scrapes all electrons above a certain value and accelerates them to very high velocities of $v\simeq 6v_e$.

The main consequence is that the number of fast electrons may increase considerably because of this scraping effect. At lower densities, the wave-particle interactions extend closer to the bulk of the distribution, and a larger electron population will be trapped and further accelerated by the propagating wave.

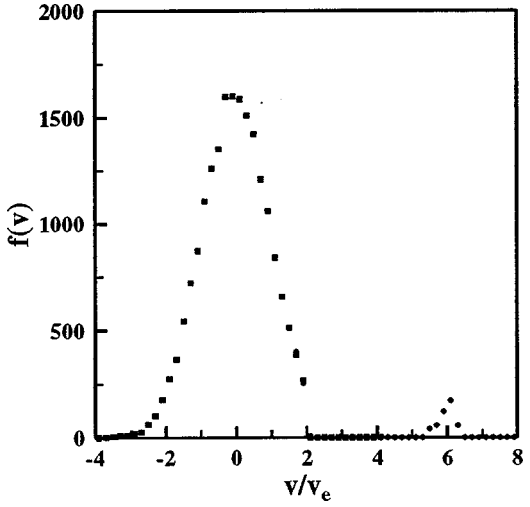

FIG. 3. Final velocity distribution of the electrons behind the cutoff layer obtained for an initially Maxwellian ensemble of test electrons in the case shown in Fig. 2.

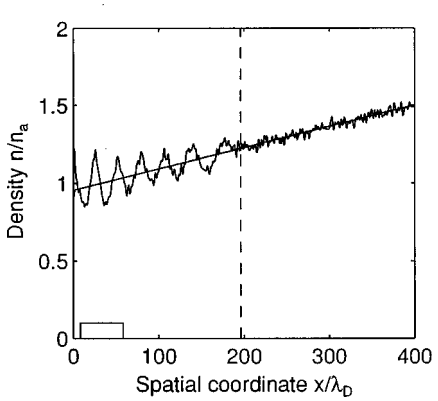

FIG. 4. The electron and ion densities, when an electron plasma wave arrives at the critical layer. The square on the x axis indicates the location of the external antenna, and the dashed line shows the cutoff layer of the excited plasma wave. Because of the fixed ions, the density profile does not change during the simulation.

IV. PARTICLE-IN-CELL SIMULATIONS

The interesting properties of the fast electron generation that were found above were also investigated with the one-dimensional bounded electrostatic particle-in-cell simulation code XPDP1 [11,12]. The code was modified to excite the electron plasma wave by an external oscillating charge of the standing wave form $\rho_0(x)\sin(kx)\cos(\omega t)$, where $\rho_0(x)$ is localized close to the low density boundary. In the present simulation, the width of the antenna was two wavelengths.

In the PIC simulation described below, the frequency of the plasma wave was $\omega = 1.106\omega_{p0}$, where ω_{p0} denotes the plasma frequency at the location of the antenna. The wave number launched by the antenna was $k_0\lambda_{D0} = 0.25$, where λ_{D0} refers to the Debye length at the location of the antenna. The wave number is low enough in the low density side of the plasma slab to allow the wave propagation up the density gradient. The distance between the center of the antenna and the cutoff layer was $\ell = 163\lambda_{D0}$, and the cutoff layer was located at $x_c = 196\lambda_{D0}$. The scale length of the inhomogeneity was $n_{e0}/n'_{e0} = 734\lambda_{D0}$, where n_{e0} and n'_{e0} are the density and its derivative at the antenna, respectively. A fixed ion background was assumed. The simulation geometry and the density profile are illustrated in Fig. 4, which shows the locations of the antenna and the cutoff surface.

A generic problem of PIC simulations is the high noise level caused by the fairly small number of discrete particles. The noise level reduces with increasing number of macroparticles, which in the present simulation was 210 particles per cell corresponding to the total number of 315 000 electrons and ions. In order to reduce effects caused by the high density boundary, the simulation box was chosen to extend well beyond the cutoff layer. The total length of the simulation box was $L = 653\lambda_{D0}$. To keep the noise level low enough, fairly intense plasma waves were generated in the present simulation. Consequently, a perturbation in the charge density having an amplitude of about 1.8% of the background ion charge density was used as an antenna.

Figure 5 illustrates the penetration of an electron plasma wave towards the cutoff layer. The electrostatic field is shown at two different instants: $\omega_{p0}t = 82$ and 353. Figure 5(b) shows the wave when it has reached the cutoff surface, and the Airy-type pattern starts to form. The increase in the phase velocity due to the increasing wavelength can be seen near the cutoff layer. The wave cannot propagate in the evanescent region behind the cutoff and thus the noise level can be evaluated from the right-hand side of the cutoff layer.

The noise can be further reduced from the signals by using so-called interferograms which show the temporal correlation between a sinusoidal reference signal and an electrostatic wave. Following Abe and Itatani [13] we define the interferograms as

$$E_s(x,t) = \frac{2}{\tau_c}\int_{t-\tau_c}^{t} \sin(\omega\tau)E(x,\tau)d\tau, \tag{6}$$

$$E_c(x,t) = \frac{2}{\tau_c}\int_{t-\tau_c}^{t} \cos(\omega\tau)E(x,\tau)d\tau, \tag{7}$$

where ω is the frequency of the antenna, and the correlation time τ_c was typically chosen to be a few periods of the wave. An interferogram of the field is shown in Fig. 5(c), where we have chosen $\omega\tau_c = 8\pi$. The decrease of the noise level behind the cutoff layer is quite clear.

The interferograms are applied to study the dispersion characteristics of the plasma wave in an inhomogeneous plasma. The wave number and the phase velocity of the electron plasma wave in the density ramp were measured by determining the phase of the wave from the interferograms defined in Eqs. (6) and (7). First, the phase of the wave was calculated from

$$\Theta(x) = \arctan\left(\frac{E_c(x,t)}{E_s(x,t}\right). \tag{8}$$

The wave number is then

$$k(x) = \frac{\Delta\Theta}{\Delta x}, \tag{9}$$

and the phase velocity is obtained from $v_{\rm ph}(x) = \omega/k(x)$. The numerical differentiation in Eq. (9) was performed by fitting

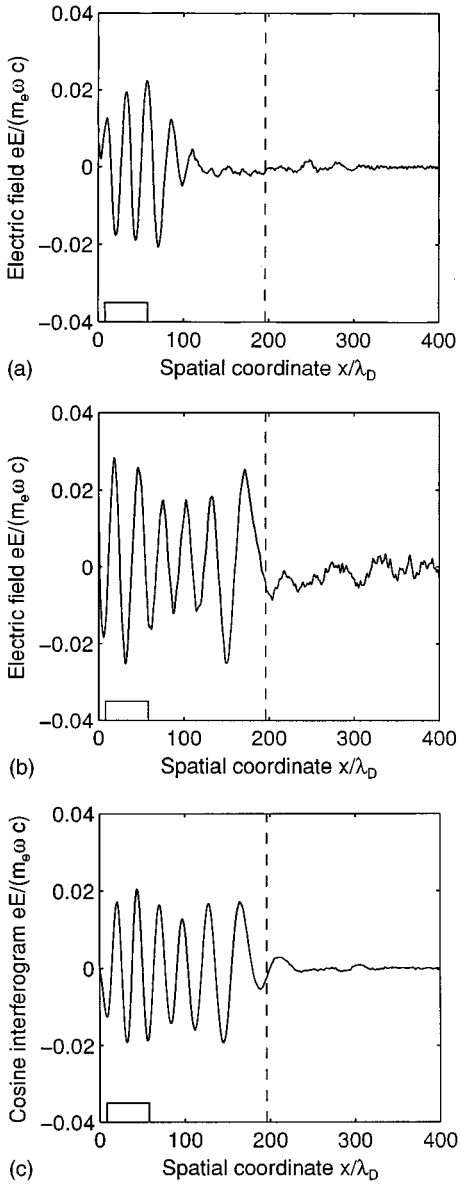

FIG. 5. Electric field of the propagating electron plasma wave in an inhomogeneous density profile at time (a) $\omega_{p0}t=82$ and (b) $\omega_{p0}t=353$. The corresponding interferogram is shown at time (c) $\omega_{p0}t=353$.

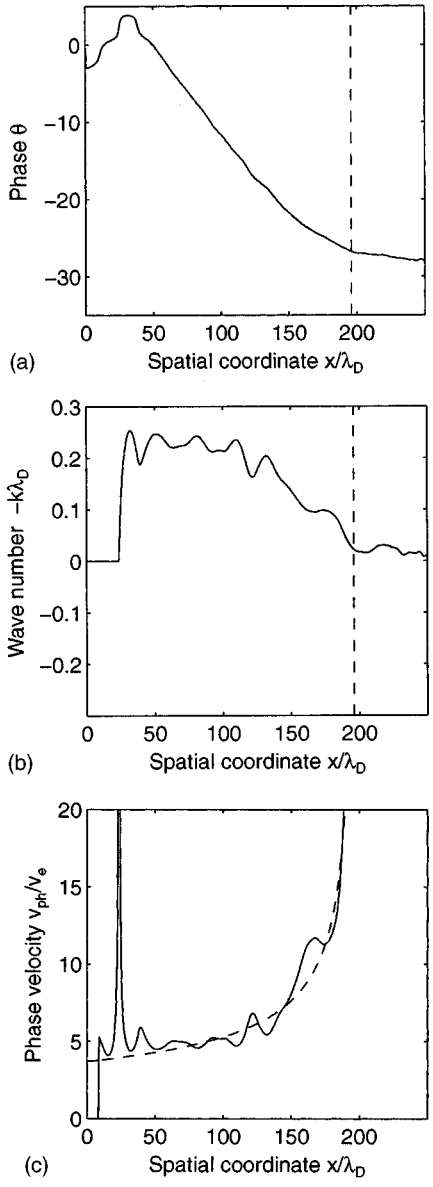

FIG. 6. Measurement of the phase velocity in the PIC simulation. (a) The phase factor obtained from the interferograms. (b) The wave number obtained by differentiation. (c) The corresponding phase velocity; the dashed curve is the estimate obtained from the Bohm-Gross dispersion relation ($\omega_{p0}t=353$, $\omega\tau_c=8\pi$).

a straight line to 50 values of $\Theta(x_i)$ by the method of least squares, and by calculating the slope of the line. This method was found to reduce noise and oscillation in the derivative.

The phase of the wave in Fig. 5 is shown in Fig. 6(a). The slope of the phase decreases near the cutoff layer, and correspondingly the magnitude of the wave number also decreases, see Fig. 6(b). The phase velocity is shown in Fig. 6(c), and the phase velocity obtained from the Bohm-Gross dispersion relation is shown by a dashed line. The agreement between these two curves is surprisingly good.

In the above analysis, the WKB approximation is used, and it breaks down near the cutoff layer. The maximum phase velocity of the wave shown in Fig. 5 should be estimated from Eq. (5). The result is $v_{\rm ph}(x_c)/v_{\rm ph}(x_0)=1.93$, where x_0 denotes the location of the center of the antenna. This corresponds to $v_{\rm ph}(x_c)=8.5v_e$, which should be kept in mind in the interpretation of Fig. 6(c). Direct measurement of the last half wavelength in Fig. 5(c) gives the maximum phase velocity $v_{\rm ph}(x_c)=8.7v_e$, which is in good agreement with the above analysis.

The increase of the phase velocity near the cutoff surface is found to be similar to the test particle simulations described in Sec. III. Therefore somewhat similar generation and acceleration of fast electrons can be expected in the PIC simulation.

V. FAST ELECTRON GENERATION IN PIC SIMULATIONS

A basic difficulty with PIC simulations is that there are only a few particles in the tail of a Maxwellian velocity

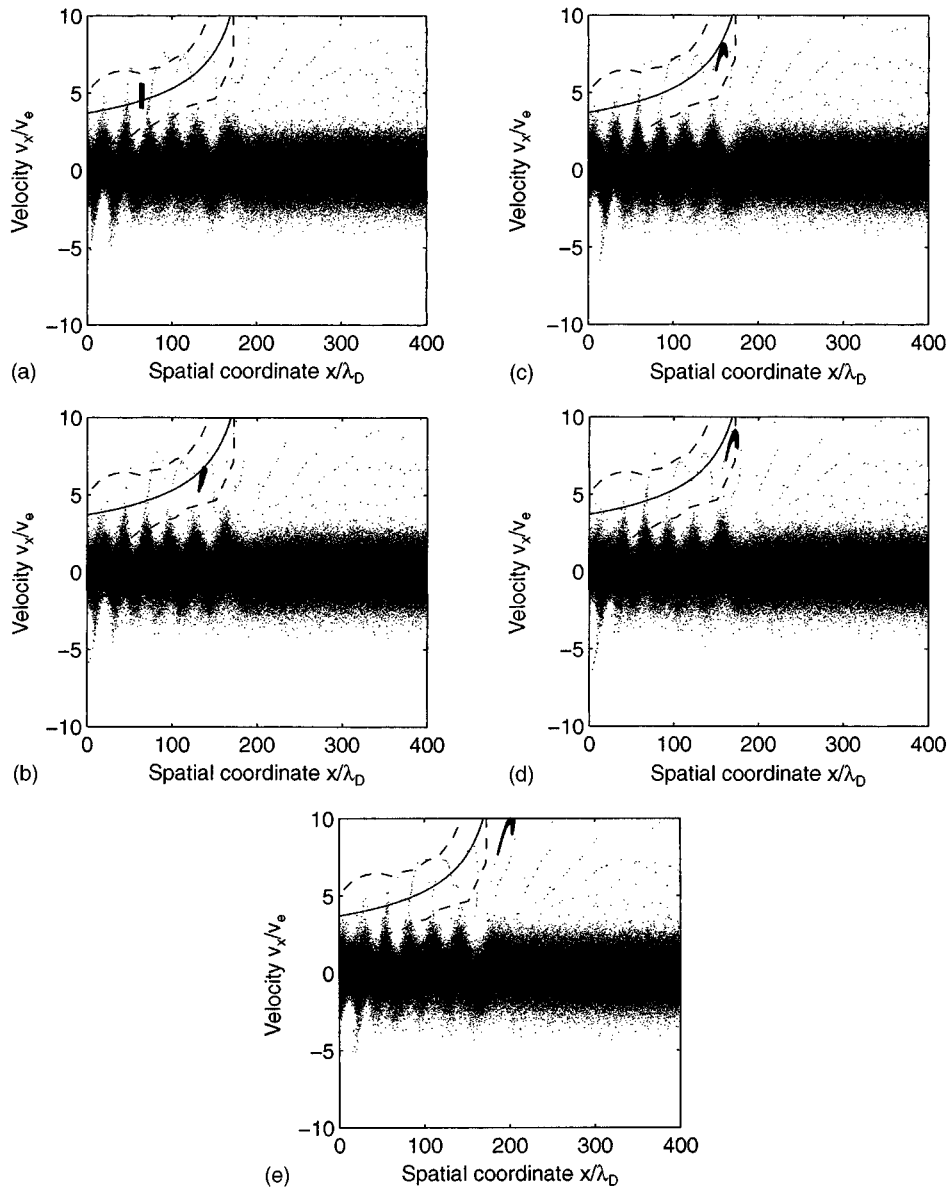

FIG. 7. Phase-space plot including a test electron ensemble for the fast electron diagnostics. The test electrons start to move at (a) $\omega_{p0}t=329$, and the following four figures show the propagation of the ensemble at (b) $\omega_{p0}t=345$, (c) 348, (d) 350, and (e) 353. The solid curve shows the phase velocity estimated from the Bohm-Gross dispersion relation, and the dashed curves show the trapping widths.

distribution. This problem was circumvented by following an ensemble of test particles moving in the self-consistent field obtained from the PIC simulation. A similar idea has previously been applied to Vlasov simulations by Ghizzo *et al.* [14]. The test electrons experience the self-consistent field of plasma particles but their effect on the field is not taken into account. Since the test particles do not contribute to the background field, they do not generate any artificial instabilities. The test particles can be loaded to any volume in the phase space, and they can be let free at any time during the simulation. This is a valuable tool for PIC simulations of the tail phenomena which often suffer from poor statistics.

In the PIC simulation, the phase-space behavior of two ensembles of 20 000 test electrons was followed. The test electrons were let free at time $\omega_{p0}t=329$ when the electron plasma wave was fully developed. The initial velocities of the test electrons were evenly distributed between $4.1v_e$ and $5.6v_e$, which is just above the local phase velocity. Initially, the test electron ensemble was located just on the right-hand side of the antenna to avoid direct acceleration by the antenna itself. The spatial width of the ensemble was $0.131\lambda_0$, where λ_0 is the wavelength of the plasma wave at the center of the antenna. The test electrons are seen as a black rectangle in Fig. 7(a), where the phase velocity of the wave estimated from the Bohm-Gross dispersion relation is shown by the solid curve. The trapping width calculated from the wave envelope at time $\omega_{p0}t=353$ is shown by dashed lines.

In Fig. 7, the acceleration of the test electrons when they approach the cutoff layer is shown in detail. The electrons follow the increasing phase velocity of the wave quite accurately. When they arrive at the cutoff layer at $x_c=196\lambda_{D0}$, they are detrapped from the wave potential and start to stream freely in the region where the wave cannot penetrate.

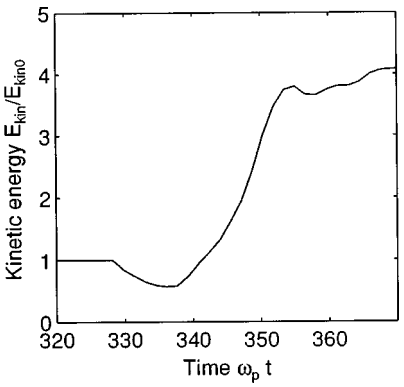

FIG. 8. The time evolution of the average kinetic energy of the test particle ensemble shown in Fig. 7.

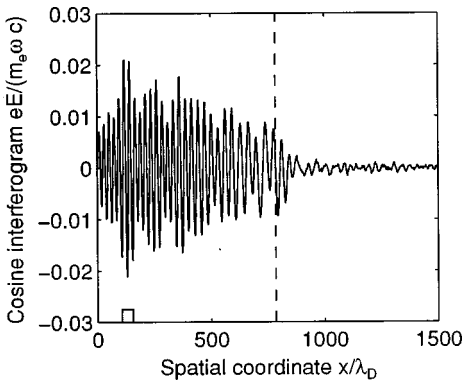

FIG. 9. Interferogram of the wave amplitude in the gentle density gradient at time $\omega_{p0}t=1643$.

At this point their velocities are between $7v_e$ and $10v_e$, which is in agreement with the maximum phase velocity of $v_{\rm ph}(x_c)=8.5v_e$ calculated in the end of Sec. IV.

The trapping width around the phase velocity for the electrons is given as $v_{\rm tr}=|2q_eE/km_e|^{1/2}$. In the present simulations, a typical electric field just behind the antenna is about $|q_eE|/m_e\omega c=0.025$, which corresponds to the trapping width of $v_{\rm tr}=2.3v_e$ and the upper limit of $6.7v_e$ for the trapped electrons. The test electrons reach, however, much higher velocities up to $10v_e$, and therefore the acceleration is caused by the increasing phase velocity near the cutoff layer.

The phase-space plots in Fig. 7 also show some acceleration of background electrons and generation of a small population of fast background electrons. The amplitude of the antenna is large enough to trap some thermal electrons from the background distribution even though PIC codes without test particles have a fairly poor resolution in the tail phenomena.

The time evolution of the kinetic energy of the test electrons is shown in Fig. 8. The kinetic energy of the test population has increased roughly by a factor of 4 when the electrons arrive at the cutoff layer at time $\omega_{p0}t\simeq 353$. After this, the kinetic energy remains almost constant because the test particles have moved behind the cutoff surface where there is no electron plasma wave accelerating them. In the end of Sec. IV, we estimated that the enhancement of the phase velocity is $v_{\rm ph}(x_c)/v_{\rm ph}(x_0)=1.9$, which corresponds to enhancement of the kinetic energy by a factor of 3.7. This is in fairly good agreement with the result shown in Fig. 8.

VI. EFFECT OF THE STEEPNESS OF THE DENSITY GRADIENT

According to the simple scaling law in Eq. (5), there are two factors that affect the enhancement of the velocity of the trapped electrons in a linear density gradient; first, the phase velocity (or the wave number) in the region where the electron plasma wave is generated; second, the distance from this region to the cutoff layer, i.e., the magnitude of the density gradient. In the following, we investigate the effect of the density gradient on the fast electron generation by repeating the above simulation in a plasma with a gentle density gradient and in a homogeneous plasma.

In the simulation with a gentle density gradient, the wave parameters at the antenna were the same as in the simulation discussed above (i.e., $k_0\lambda_{D0}=0.25$). The distance between the antenna and the cutoff layer, however, was $\ell=661\lambda_{D0}$, which is approximately by a factor of 4 larger than in the previous simulation. Therefore the scale length of the inhomogeneity also was larger: $n_{e0}/n'_{e0}=2937\lambda_{D0}$. According to Eq. (5), the expected enhancement of the phase velocity would in this case be much larger than in the previous simulation: $v_{\rm ph}(x_c)/v_{\rm ph}(x_0)=3.1$. The number of electrons in this simulation was 1 500 000, which is 333 electrons per cell.

The electric field obtained in a gentle density gradient is illustrated in Fig. 9. In contrast to the previous simulation, the linear Landau damping is now important because we have made the distance from the antenna to the cutoff layer longer. The linear Landau damping length for the wave with $k_0\lambda_{D0}=0.25$ is $L_{LD}=313\lambda_{D0}$, where we have defined $L_{LD}=v_g/\gamma$, and γ is the imaginary part of the frequency. Since the distance from the antenna to the cutoff layer is larger by a factor of 2 than the damping length, the wave amplitude decreases near the cutoff layer.

The generation of fast electrons was again investigated by following an ensemble of test electrons that were initially located near the antenna with evenly distributed velocities between $3.5v_e$ and $4.9v_e$. The time evolution of the kinetic energy of the test electrons that were let free at time $\omega_{p0}t=1640$ is shown in Fig. 10. The increase of the kinetic energy is modest in this case because the wave is signifi-

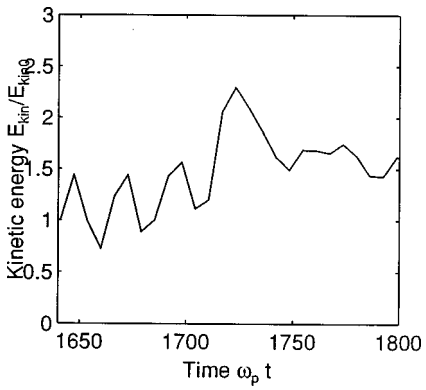

FIG. 10. The time evolution of the average kinetic energy of a test particle ensemble in the gentle density gradient.

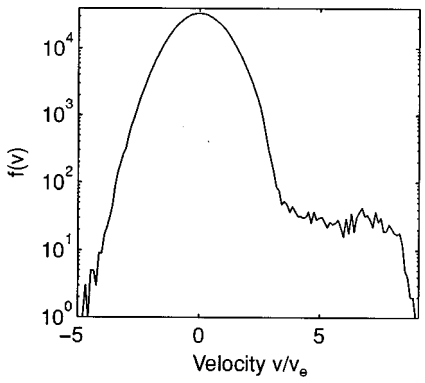

FIG. 11. Velocity distribution of the electrons in the region $496\lambda_{D0} \leqslant x \leqslant 1487\lambda_{D0}$ at time $\omega_{p0}t = 1643$ in the gentle density gradient.

cantly damped before the cufoff layer. Therefore a large part of the electrons becomes detrapped before they are accelerated.

Some generation of the fast background electrons occurs in this case because of the Landau damping of the wave. At time $\omega_{p0}t = 1643$, a plateau is formed in the velocity distribution of the background electrons as is shown in Fig. 11. Note that the fast electrons generated in the underdense plasma travel to the region behind the cutoff layer with velocity that is approximately equal to the phase velocity of the wave. Therefore the velocity distribution has been plotted for the region $496\lambda_{D0} \leqslant x \leqslant 1487\lambda_{D0}$.

In a homogeneous plasma, the acceleration caused by the increasing phase velocity should disappear. The Landau damping of the wave launched into a homogeneous plasma with wave number $k_0\lambda_{D0} = 0.25$ is illustrated in Fig. 12. The test electrons were again initially located near the antenna with velocities between $3.5v_e$ and $4.9v_e$, and they were let free at time $\omega_{p0}t = 2300$. As was expected, their energy did not increase when they traveled through the simulation box, as can be seen from Fig. 13.

VII. A PHENOMENOLOGICAL MODEL FOR THE ''DRAG DAMPING''

In the test particle calculations of Sec. III and PIC simulations of Secs. V and VI, some of the electrons were trapped in the potential well of a wave with increasing phase velocity. Since these electrons were found to gain energy, the wave must be damped. In the following, we will present a phenomenological model for this damping mechanism, which we will call ''drag damping'' because the wave with an increasing phase velocity drags the electrons to higher velocities.

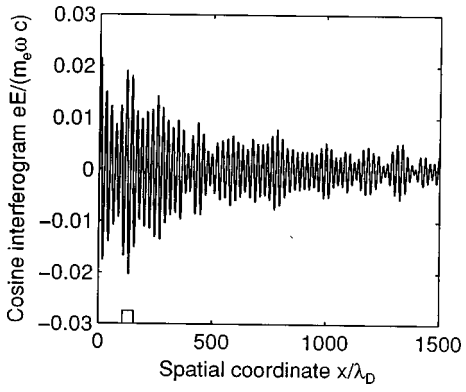

FIG. 12. Interferogram of the wave amplitude in a homogeneous plasma at time $\omega_{p0}t = 2137$.

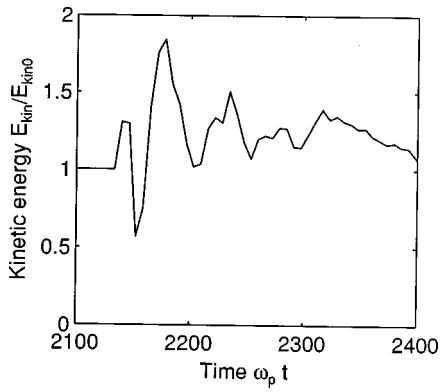

FIG. 13. The time evolution of the average kinetic energy of a test particle ensemble in a homogeneous plasma.

A. ''Drag damping'' of a Langmuir wave

Consider a wave with a slowly varying amplitude and wave number:

$$\mathcal{E}(x,t) = E(x)\cos[k(x)x - \omega t]. \tag{10}$$

Energy flux of the wave is $S_w(x) = v_g(x)W(x)$, where the energy density is

$$W(x) = \frac{1}{4}\varepsilon_0\left[1 + \frac{\omega_p^2(x)}{\omega^2}\right]E^2(x). \tag{11}$$

We first consider the propagation of the wave in the absence of damping. In steady state, we must then have constant energy flux $S_w(x)$ in the region $0 \leqslant x \leqslant x_c$. We can solve for the wave amplitude, which is

$$E_{\mathrm{ND}}^2(x) = E_0^2\left(\frac{u_0}{u(x)}\right)^3 \frac{2u_0^2 - 3}{2u^2(x) - 3}, \tag{12}$$

where the subscript ''ND'' stands for ''no damping,'' and E_0 is the wave amplitude at $x = 0$. The normalized phase velocities are

$$u(x) \equiv \frac{v_{\mathrm{ph}}(x)}{v_e} = \left(\frac{3n_c}{n_c - n_e(x)}\right)^{1/2}, \tag{13}$$

$$u_0 \equiv \frac{v_{\mathrm{ph}}(0)}{v_e} = \left(\frac{3n_c}{n_c - n_0}\right)^{1/2}, \tag{14}$$

where n_0 and n_c refer to the electron densities at $x = 0$ and at the cutoff layer, respectively.

With the aid of Eqs. (13) and (14) the amplitude in Eq. (12) can be written as

$$E_{\mathrm{ND}}^2(x) = E_0^2\left(\frac{n_c - n_0}{n_c - n_e(x)}\right)^{1/2}\left(\frac{n_c + n_0}{n_c + n_e(x)}\right). \tag{15}$$

In a linear density gradient, we obtain

$$E_{\mathrm{ND}}^2(x)=E_0^2\left(1+\frac{n_c-n_0}{n_c+n_0}\frac{x}{x_c}\right)^{-1}\left(1-\frac{x}{x_c}\right)^{-1/2}. \quad (16)$$

Equations (12)–(16) describe the enhancement of the wave amplitude when the group velocity decreases near the cutoff layer.

Consider next those electrons that are trapped and travel with the wave when the phase velocity increases. Averaging over the bounce motion of the electrons we find that their energy flux is

$$S_p(x)=\frac{1}{2}n_{\mathrm{tr}}m_e v_{\mathrm{ph}}^3(x), \quad (17)$$

where n_{tr} is the density of the trapped electrons traveling with the wave. For simplicity, we shall assume that the density of the trapped electrons is constant, i.e., it does not depend on x. This assumption is valid only if the wave amplitude does not vary too much during the propagation. We can then estimate

$$n_{\mathrm{tr}}=n_0\int_{v_{\mathrm{ph}}(0)-v_{\mathrm{tr}}(0)}^{v_{\mathrm{ph}}(0)+v_{\mathrm{tr}}(0)} f(v)dv, \quad (18)$$

where v_{tr} is the average trapping width.

When $f(v)$ is the Maxwellian distribution, the integral in Eq. (18) can be written in terms of the error function:

$$n_{\mathrm{tr}}=\frac{1}{2}n_0\left[\mathrm{erf}\left(\frac{u_0}{\sqrt{2}}+\sqrt{u_0w_0}\right)-\mathrm{erf}\left(\frac{u_0}{\sqrt{2}}-\sqrt{u_0w_0}\right)\right], \quad (19)$$

where the normalized oscillation velocity is

$$w_0\equiv\frac{v_{\mathrm{osc}}(0)}{v_e}=\frac{eE_0}{m_e\omega v_e}. \quad (20)$$

In the limit of a small trapping width ($v_{\mathrm{tr}}/v_e=\sqrt{2u_0w_0}\ll u_0$), we obtain by the Taylor expansion the expected result:

$$n_{\mathrm{tr}}\simeq 2n_0 f(v_{\mathrm{ph}}(0))v_{\mathrm{tr}}(0)=\frac{2n_0}{\sqrt{\pi}}(u_0w_0)^{1/2}\exp(-u_0^2/2). \quad (21)$$

Since some of the electrons are accelerated with the increasing phase velocity, they must obtain energy from the wave. Therefore, the wave must be damped. Let us assume for a while that all other damping mechanisms can be neglected. In steady state, we then have

$$S_w(x)+S_p(x)=\text{ const.} \quad (22)$$

Solving again for the amplitude we obtain

$$E^2(x)=E_{\mathrm{ND}}^2(x)R_D(x), \quad (23)$$

where the damping factor is

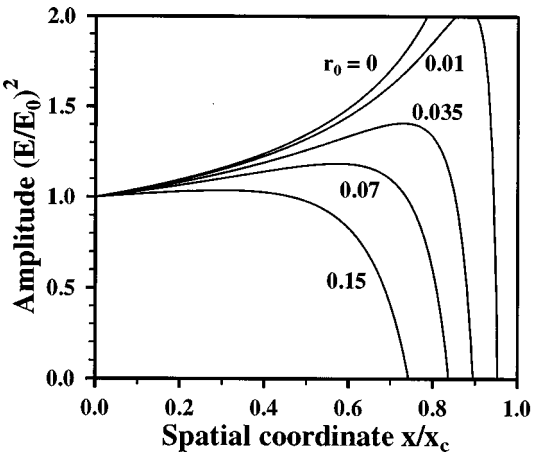

FIG. 14. The wave amplitude near the critical layer, when the trapping factor is $r_0=0$, 0.01, 0.035, 0.07, 0.15. Only drag damping is taken into account ($k_0\lambda_{D0}=0.25$, $n_0/n_c=0.82$).

$$R_D(x)=1-\frac{S_p(x)-S_p(0)}{S_w(0)}. \quad (24)$$

Note that we obtain the nondamped result in Eq. (15) if no electrons are accelerated with the wave, i.e., $S_p(x)\equiv S_p(0)$.

The damping factor can be written as

$$R_D(x)=1-r_0\left[\left(\frac{u(x)}{u_0}\right)^3-1\right], \quad (25)$$

where r_0 is the initial ratio of the energy fluxes: $r_0=S_p(0)/S_w(0)$. In a linear density gradient, we obtain

$$R_D(x)=1-r_0\left[\left(1-\frac{x}{x_c}\right)^{-3/2}-1\right]. \quad (26)$$

The factor r_0 is obtained for any density profile with the aid of Eqs. (11) and (17). We find

$$r_0=\frac{2}{3}\frac{u_0^4}{w_0^2}\frac{u_0^2-3}{2u_0^2-3}\frac{n_{\mathrm{tr}}}{n_0}, \quad (27)$$

where n_{tr} is given by Eq. (19) or (21). By using the Bohm-Gross dispersion relations in Eqs. (13) and (14), the damping factor in Eqs. (25)–(27) can be written in terms of the densities:

$$r_0=\frac{6}{w_0^2}\left(1-\frac{n_0}{n_c}\right)^{-2}\left(1+\frac{n_c}{n_0}\right)^{-1}\frac{n_{\mathrm{tr}}}{n_0}. \quad (28)$$

The effect of drag damping on the wave amplitude is illustrated in Fig. 14 for different amounts of trapped electrons traveling with the wave. In the undamped case ($r_0=0$), the amplitude obtained from the WKB calculation diverges near the cutoff layer. When the energy of the trapped electrons is a few percent of the wave energy, the wave is significantly damped near the cutoff layer.

Since the phase velocity obtained from the WKB approximation approaches infinity near the cutoff layer, Eqs. (25) and (26) overestimate the strength of the effect. The acceleration of the electrons and the damping stops at the point

where the phase velocity achieves its maximum value given in Eq. (5). In WKB approximation, this phase velocity is achieved at

$$\frac{x_{\max}}{x_c} \simeq 1 - 0.31(k_0 x_c)^{-2/3}. \tag{29}$$

Taking the parameters of the PIC simulation in Sec. V, we obtain $x_{\max}/x_c \simeq 0.97$.

Note that in the derivation of drag damping we have used very general energy conservation arguments which apply to any slowly varying density profile. The only limitation is the WKB approximation in Eq. (10).

B. Comparison with the Landau damping

Drag damping is important only in situations where it is stronger than other damping mechanisms. In the following, we compare drag damping with the linear Landau damping.

Assume for a while that the linear Landau damping is the only damping mechanism. Then Eq. (23) should be replaced by

$$E^2(x) = E_{\mathrm{ND}}^2(x) R_L(x), \tag{30}$$

where

$$R_L(x) = \exp[2I(x)], \tag{31}$$

$$I(x) = \int_0^x k_i(\zeta)\, d\zeta. \tag{32}$$

The imaginary part of the wave number is $k_i(x) = \gamma(x)/v_g(x)$, where γ is the imaginary part of the frequency.

At small values of the wave number ($k\lambda_D \lesssim 0.25$), the damping decrement can be approximated as

$$\gamma(x) = -\frac{1}{2}\sqrt{\frac{\pi}{2}} \frac{\omega_p^4(x)}{k^3(x) v_e^3} \exp[-u(x)^2/2]. \tag{33}$$

In Eq. (33), we approximate $\omega_p^4(x) \simeq \omega^4$, which overestimates the Landau damping. The imaginary part of the wave number is then

$$k_i(x) = -\frac{1}{6}\sqrt{\frac{\pi}{2}} \lambda_{D,c}^{-1} u^4(x) \exp[-u^2(x)/2], \tag{34}$$

where $\lambda_{D,c}$ is the Debye length at the cutoff layer.

With the aid of the Bohm-Gross dispersion relation, we now obtain

$$I(x) = -\frac{1}{2}\sqrt{\frac{\pi}{2}} \frac{n_c}{\lambda_{D,c}} \int_{u_0^2}^{u^2(x)} \frac{1}{n_e'(x)} \exp(-z/2)\, dz. \tag{35}$$

If we assume that the spatial derivative of the density does not vary too much [$n_e'(x) = \mathrm{const}$], we can take it outside the integral. We then obtain

$$I(x) \simeq -\sqrt{\frac{\pi}{2}} \left(\frac{n_c}{n_e'(x_c)\lambda_{D,c}} \right) \{ \exp[-u^2(x)/2] - \exp[-u_0^2/2] \}, \tag{36}$$

which can again be written in terms of the densities by using Eqs. (13) and (14).

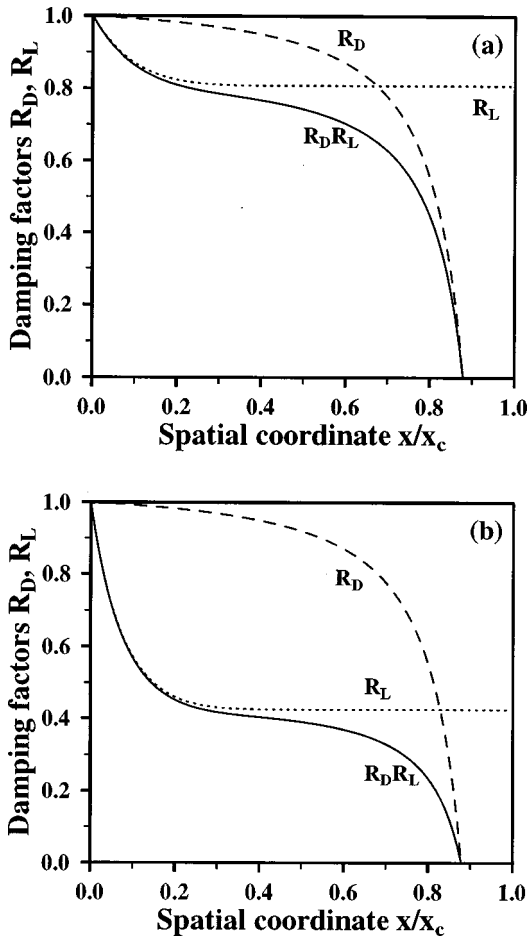

FIG. 15. Damping factors near the critical layer in steep and gentle density gradients. Effects of drag damping (dashed line), Landau damping (dotted line), and their combination (solid line) are shown when the length of the plasma is (a) $x_c/\lambda_{D,c} = 180$, (b) $x_c/\lambda_{D,c} = 720$ ($k_0\lambda_{D0} = 0.25$, $r_0 = 0.044$).

Drag damping can be considered important when the damping factor in Eq. (25) is of the same order as the Landau damping factor in Eq. (31). Often we will have both damping mechanisms present, and instead of Eqs. (23) and (30) we have to estimate the amplitude from

$$E^2(x) = E_{\mathrm{ND}}^2(x) R_D(x) R_L(x). \tag{37}$$

The damping factors in linear Landau damping and drag damping are illustrated in Fig. 15 for steep and gentle density gradients. The linear Landau damping is important only in the low density region where the wave number is close to its initial value $k_0\lambda_{D0} = 0.25$. When the wave has propagated in the high density region and the wave number is small enough ($k\lambda_{D0} < 0.20$), no damping occurs any more. In the steep density gradient of Fig. 15(a), the region where Landau damping is important (i.e., $k\lambda_{D0} > 0.20$) is so short that the damping factor saturates at the level of $R_L \simeq 0.8$. In the gentle

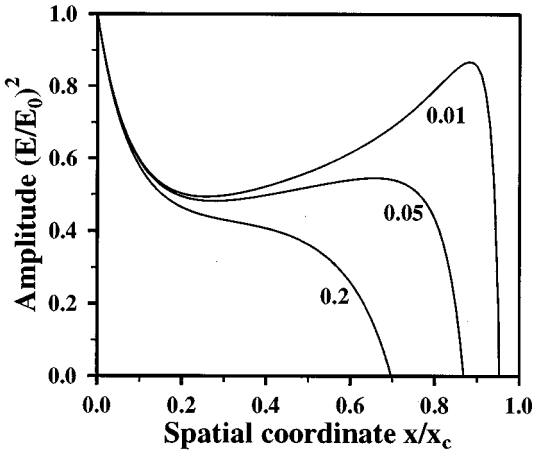

FIG. 16. The wave amplitude near the critical layer, when the trapping factor is $r_0=0.01$, 0.05, 0.2. Both drag and Landau damping are taken into account ($k_0\lambda_{D0}=0.25$, $n_0/n_c=0.82$, $x_c/\lambda_{D,c}=720$).

density gradient of Fig. 15(b), Landau damping is efficient in a longer region and the saturation level is $R_L\simeq 0.4$.

In Fig. 15, the drag damping is most efficient near the cutoff layer where the damping factor R_D decreases to zero in both cases. The total damping given by the product of the damping factors $R_L R_D$ is dominated by the Landau damping in the low density region and by the drag damping near the cutoff layer. In a gentle density gradient, only a small amount of energy is left in the wave to accelerate electrons near the cutoff layer because most of the energy is already absorbed in the low density region.

The steep density gradient in Fig. 15(a) is similar to the density gradient of the simulations in Secs. IV and V, where strong generation of fast electrons near the cutoff layer was found. The result in Fig. 15(a) is in qualitative agreement with the results of the PIC simulations because the drag damping is the dominating damping mechanism. The gentle density gradient in Fig. 15(b) corresponds to the density gradient in Sec. VI, where the generation of fast electrons was found to be weak. This is again in qualitative agreement with the result shown in Fig. 15(b), where the wave is damped mainly by linear Landau damping.

The wave amplitude obtained from Eq. (37) is illustrated in Fig. 16 in the case of a gentle density gradient. In the low density region, the linear Landau damping is the dominating effect. At medium densities, the Airy swelling caused by the decreasing group velocity starts to be important. Near the critical layer, the drag damping dominates.

VIII. SUMMARY AND DISCUSSION

Particle-in-cell simulations of fast electron generation by a propagating electron plasma wave in an inhomogeneous plasma have been performed. The density profile was taken linear so that the phase velocity of the electrostatic plasma wave varied locally. Self-consistent PIC simulations were complemented by simple test particle calculations with a prescribed electrostatic wave having a form of the Airy function.

The simulations show clearly that the electrons trapped into the wave potential at lower densities travel trapped with the wave, and are further accelerated when the plasma density and the phase velocity of the wave increase. This leads to considerably higher electron energies than in a homogeneous plasma where the phase velocity is constant and the upper limit of the electron velocity is determined by the trapping width in velocity. The enhancement of the phase velocity and the velocity of the trapped electrons was found to be approximately $v_{\rm ph}(x_c)/v_{\rm ph}(0)\simeq 0.56(k_0x_c)^{1/3}$, where x_c is the length of the underdense plasma and k_0 is the initial wave number.

PIC simulations were performed in both steep and gentle density gradients. In a steep density gradient, the trapped electrons were found to follow the increasing phase velocity of the wave. Behind the cutoff layer, the velocities of the accelerated electrons were found to be in rough agreement with the enhanced phase velocity obtained from the formula given above. Novel test particle diagnostics were used in the PIC simulations to follow the acceleration of an ensemble of trapped test electrons through the cutoff layer.

In a gentle density gradient, the linear Landau damping was found to be important because the Landau damping length $L_{\rm LD}=v_g/\gamma$ was small compared to the length of the underdense plasma, i.e., $L_{\rm LD}\lesssim x_c$. Since the wave was already damped when it reached the cutoff layer, the generation of fast electrons was not very strong.

Note that in the calculations presented above the initial wave number was $k_0\lambda_{D0}=0.25$. If a smaller wave number had been chosen, for instance, $k_0\lambda_{D0}=0.20$, the linear Landau damping would not have been important even in fairly gentle density gradients. This could make it possible to obtain acceleration also in these cases. Such simulations would be, however, very demanding because of the large number of particles needed in long plasmas. In addition, the small group velocity of the wave with a small wave number would lead to very long simulations.

Since the electrons trapped in the wave potential were found to gain energy, the wave must be damped. We have called this damping mechanism drag damping because the wave with an increasing phase velocity drags the electrons to higher velocities. A phenomenological model for the drag damping was presented which describes the energy balance between the wave and the accelerating electrons in a steady state. The strength of the drag damping was compared with the linear Landau damping which was found to dominate in gentle density gradients if the initial wave number is large ($k_0\lambda_{D0}\gtrsim 0.22$). The phenomenological model was found to be in a qualitative agreement with the PIC simulations. The model could be improved by taking into account that the changes in the wave amplitude lead to changes in the trapping width and in the number of the trapped electrons. This improvement would lead to a set of coupled differential equations describing the wave-particle interaction near the cutoff layer.

The present test particle model and the PIC simulations are relevant to the nonlinear laser-plasma interactions in the underdense plasma region where large amplitude Langmuir waves are generated by parametric instabilities. The analysis

shows that the fast electron properties may change considerably in the presence of a density gradient as is the case in any realistic conditions. The main result is that the number of very fast electrons may increase substantially because at lower densities the wave-particle interaction takes place closer to the bulk electrons, and the trapped particles will be further accelerated by the propagating wave.

ACKNOWLEDGMENTS

T.J.H.P. and R.A.C. are grateful to SILASI, the European TMR Network on SuperIntense LAser pulse-Solid Interaction, on creating fruitful collaboration. We would like to thank the Plasma Theory and Simulation Group (Professor C.K. Birdsall, University of California, Berkeley) for providing us with their 1d3v PIC code XPDP1.

[1] T. Tajima and J. M. Dawson, Phys. Rev. Lett. **43**, 267 (1979).
[2] B. I. Cohen, R. H. Cohen, B. G. Logan, W. McCay Nevins, G. R. Smith, A. V. Kluge, and A. H. Kritz, Nucl. Fusion **28**, 1519 (1988).
[3] S. J. Karttunen, T. J. H. Pättikangas, R. R. E. Salomaa, and S. K. Sipilä, Nucl. Fusion **31**, 1079 (1991).
[4] P. T. Bonoli and R. C. Englande, Phys. Fluids **29**, 2937 (1986).
[5] P. Bertrand, A. Ghizzo, S. J. Karttunen, T. J. H. Pättikangas, R. R. E. Salomaa, and M. Shoucri, Phys. Rev. E **49**, 5656 (1994).
[6] P. Bertrand, A. Ghizzo, S. J. Karttunen, T. J. H. Pättikangas, R. R. E. Salomaa, and M. Shoucri, Phys. Plasmas **2**, 3115 (1995).
[7] A. Bergmann, S. Schüller, P. Mulser, and H. Schnabel, Europhys. Lett. **14**, 661 (1991).
[8] N.G. Denisov, Zh. Éksp. Teor. Fiz. **31**, 609 (1956) [Sov. Phys. JETP **4**, 544 (1957)].
[9] P. Mulser and C. van Kessel, J. Phys. D **11**, 1085 (1978).
[10] *Handbook of Mathematical Functions*, edited by M. Abramowitz and I.A. Stegun (Dover, New York, 1970), p. 478.
[11] C.K. Birdsall and A.B. Langdon, *Plasma Physics via Computer Simulation* (IOP Publishing Ltd., Bristol, England, 1991).
[12] J. P. Verboncoeur, M. V. Alves, V. Vahedi, and C. K. Birdsall, J. Comput. Phys. **104**, 321 (1993).
[13] H. Abe and R. Itatani, Phys. Fluids **22**, 1533 (1979).
[14] A. Ghizzo, M. Shoucri, P. Bertrand, T. Johnston, and J. Lebas, J. Comput. Phys. **108**, 373 (1993).